4

Computer Simulation of Data Collection in CT

While the aim of CT is the reconstruction of real objects from their actual x-ray projections, the theoretical development of CT owes a lot to reconstruction of mathematically described objects (*phantoms*) from computer simulated projection data. The basic reason for this is that computer simulation enables us to investigate individually various phenomena that cannot be separated physically. For example, x-ray data always contain noise due to both photon statistics and scatter, but simulation can indicate the specific separate effects of noise and scatter.

As can be seen from the previous chapter, a software package capable of realistic simulation of data collection using various scanning modes has to be fairly complex. Nevertheless, a number of such packages have been written. In producing many of the figures for this book we have made repeated use of one of them, called SNARK09. (The name originates from the Lewis Carroll nonsense poem entitled "The Hunting of the Snark.") SNARK09 provides a uniform framework for implementing reconstruction algorithms and for evaluating their performance. All two-dimensional reconstruction algorithms discussed in this book, as well as a number of others, are incorporated in it. In this chapter we discuss the way SNARK09 creates test data for reconstruction algorithms.

4.1 Pictures and Digitization

It is useful at this stage to make precise a number of concepts we need in the rest of this chapter and elsewhere in the book.

When we talk about a *picture*, we assume that it has two components:

(i) the *picture region,* which is a square whose center is at the origin of the coordinate system;

(ii) a *picture function* of two variables whose value is zero outside the picture region.

Sometimes, when this leads to no confusion, we call the function in (ii) the "picture." However, identical functions may give rise to different pictures if the picture regions are different. We often refer to the value of the picture at the point (x, y) as the *density* at (x, y).

An n-element *grid* subdivides the picture region into n^2 equal squares. Each of these smaller squares is called a *pixel* (short for *picture element*).

An $n \times n$ *digitized picture* is one whose value in the interior of any pixel of an n-element grid is uniform. The $n \times n$ *digitization* of a picture is an $n \times n$ digitized picture such that the integral of the original picture over any pixel of an n-element grid is equal to the integral of the digitization over the same pixel (see Fig. 1.1). In CT, the picture region is the reconstruction region and the density of the picture at the point (x, y) is the relative linear attenuation at the effective energy of the tissue at the point (x, y).

4.2 Creation of a Phantom

We now describe how a test phantom is created in SNARK09. A test phantom is nothing but a picture on which we wish to test reconstruction algorithms or data collection methods.

The phantom is put together by superimposing a number of *elemental objects*, placed at desired positions, at desired orientations and of desired size and density. The density of the elemental objects may be negative. The density of the picture at any point is then defined as the sum of the densities associated with all the elemental objects within which the point lies. To obtain an estimate of the density within a pixel, the user specifies a number K, which has the effect that the density within a pixel is determined by averaging the values of the density at $K \times K$ uniformly-spaced points within the pixel. Thus, the density assigned to a pixel can be expressed by the sum

$$\frac{1}{K^2} \sum_{k=1}^{K^2} \sum_{j=1}^{J} \delta_{k,j} d_j, \tag{4.1}$$

where J is the number of elemental objects in the phantom, d_j is the density of the jth elemental object. $\delta_{k,j} = 1$ if the kth of the $K \times K$ points in the pixel is in the jth elemental object, and $\delta_{k,j} = 0$ otherwise. Note that the digitized picture produced by this method is only an approximation to the digitization of the phantom.

An elemental object in SNARK09 may be a rectangle, an ellipse, an isosceles triangle, or a segment or a sector of a circle. The location of an elemental object is described by five variables CX, CY, U, V, and ANG. For each type of elemental object the explanation of these variables is given by Fig. 4.1. The boundary of an elemental object is considered to be part of the object.
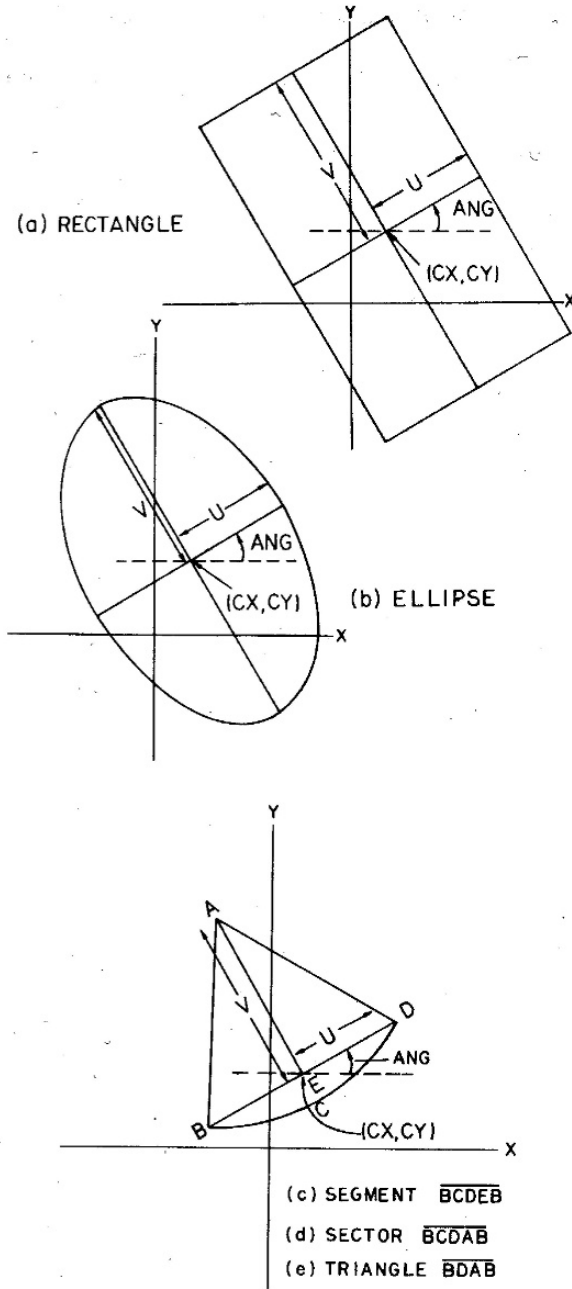
Fig. 4.1: Elemental objects. In SNARK09, an elemental object consists of both the boundary and the interior of a rectangle, or an ellipse, or a triangle, or a segment or a sector of a circle, respectively.

4.3 A Piecewise-Homogeneous Head Phantom

A most important application to date of image reconstruction from projections has been in the area of diagnostic radiology. A region of the body for which such procedures have been widely and successfully used is the head. For this reason, all ideas and methods introduced in this book are demonstrated on a typical cross section of the human head, containing tumors, a blood clot, ventricles and, of course, the skull enclosing the brain.

Our primary purpose is to introduce methods of image reconstruction from projections and to illustrate how they perform under various circumstances. Since we wish to control precisely the circumstances and to compare the results of the reconstructions with a known original, rather than using an actual cross section of a human head, we use a mathematically defined head phantom. In this and in the next section we describe how we arrived at the head phantoms that will be used repeatedly throughout the book.

We studied a cross section of a human head that was reconstructed by CT (see Fig. 4.2). Based on this cross section we described a skull enclosing the brain with ventricles, two tumors, and a hematoma (blood clot) using five ellipses, eight segments of circles, and two triangles. The tumors were placed so that they are vertically above the blood clot in the display. This facilitates reporting on our results as will be seen later on. The positioning of these ellipses, segments, and triangles is shown in Fig. 4.3.
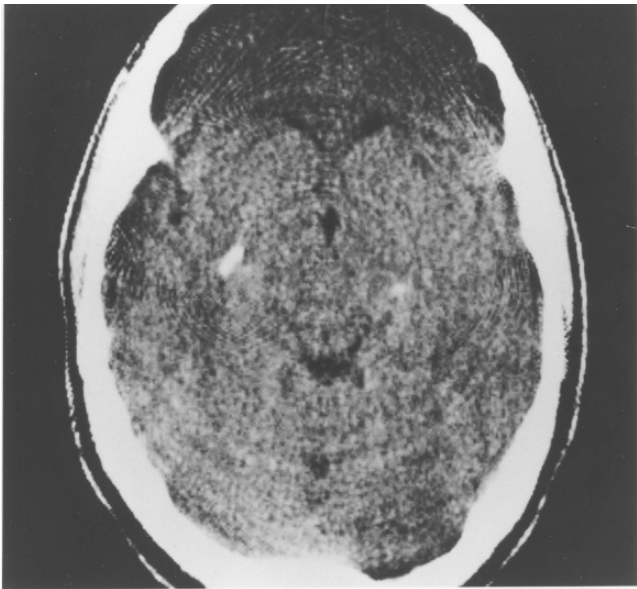

Fig. 4.2: Central part of an x-ray CT reconstruction of a cross section of the head of a patient. This served as the basis for our piecewise-homogeneous head phantom.
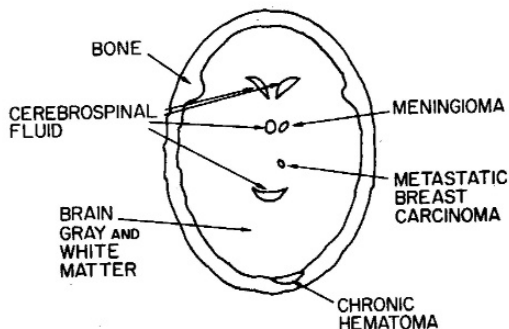
Fig. 4.3: Outlines of the elemental objects that make up the piecewise-homogeneous head phantom, with tissue type indicated for each object.

We assume that the reference material is air whose linear attenuation coefficient can be taken to be zero for all energies. Hence the density of the phantom at a point (x, y) is the linear attenuation coefficient at some fixed energy of the tissue at (x, y). Table 4.1 gives the linear attenuation coefficients of the various tissues in our head phantom at different energies. Table 4.2 gives a precise mathematical description of the location and densities of the elemental objects in Fig. 4.3, assuming 60 keV photons.

We used SNARK09 to obtain the density in each of 243×243 pixels of size 0.0752 cm with $K = 11$. The resulting array of numbers is represented in Fig. 4.4. The nature of this display deserves careful discussion. The densities given to the elemental objects were such that the resulting values are the linear attenuation coefficients at 60 keV of the appropriate tissue types measured in cm^{-1}. Thus the values range between zero (background, can be thought of as air) and 0.416 (bone of the skull). However, the interesting part of the picture is the interior of the skull. The values there range from 0.207 (cerebrospinal fluid) to 0.216 (metastatic breast tumor). The small differences between tissues inside the skull would not be noticeable if we used black to

Table 4.1: Linear attenuation coefficients (in cm^{-1}) as a function of photon energy for tissues that occur in the piecewise-homogeneous head phantom.

energy (keV)	bone	brain (gray and white matter)	metastatic breast carcinoma	meningioma	chronic hematoma	cerebro- spinal fluid
41	0.999	0.265	0.284	0.269	0.266	0.260
52	0.595	0.226	0.237	0.227	0.228	0.222
60	0.416	0.210	0.216	0.213	0.212	0.207
84	0.265	0.183	0.186	0.187	0.184	0.181
100	0.208	0.174	0.175	0.176	0.175	0.171

Table 4.2: Specifications of the elemental objects used to produce Fig. 4.4. The densities are: bone in air (Object 1), brain in bone (Object 2), cerebrospinal fluid in brain (Objects 3, 8, 10 and 12), carcinoma in brain (Object 4), meningioma in brain (Object 5), hematoma in bone (Object 6), bone in hematoma (Object 7), brain in cerebrospinal fluid (Objects 9, 11 and 13) and bone in brain (Objects 14 and 15). The word *density* here refers to differences of linear attenuation coefficients measured in cm^{-1} at 60 keV; in the polychromatic case, similar densities need to be specified for all energies in the x-ray spectrum.

No.	type	CX	CY	U	V	ANG	density
1	ellipse	0.000	0.000	8.625	6.4687	90.00	0.416
2	ellipse	0.000	0.000	7.875	5.7187	90.00	-0.206
3	ellipse	0.000	1.500	0.375	0.3000	90.00	-0.003
4	ellipse	0.675	-0.750	0.225	0.1500	140.00	0.006
5	ellipse	0.750	1.500	0.375	0.2250	50.00	0.003
6	segment	1.375	-7.500	1.100	0.6250	19.20	-0.204
7	segment	1.375	-7.500	1.100	4.3200	19.21	0.204
8	segment	0.000	-2.250	1.125	0.3750	0.00	-0.003
9	segment	0.000	-2.250	1.125	3.0000	0.00	0.003
10	segment	-1.000	3.750	1.000	0.5000	135.00	-0.003
11	segment	-1.000	3.750	1.000	3.0000	135.00	0.003
12	segment	1.000	3.750	1.000	0.5000	225.00	-0.003
13	segment	-1.000	3.750	1.000	3.0000	225.00	0.003
14	triangle	5.025	3.750	1.125	0.5000	110.75	0.206
15	triangle	-5.025	3.750	1.125	0.9000	-110.75	0.206

display zero, white to display 0.5 and corresponding grayness for values in between. In order to see clearly the features in the interior of the skull, we use zero (black) to represent the value 0.204 (or anything less) and 255 (white) to

Fig. 4.4: A piecewise-homogeneous head phantom.

represent the value 0.21675 (or anything more). This way the small change in density by 0.001 corresponds to a change of twenty in display grayness, which is visible. We used this method to produce Fig. 4.4 and the **displays of all the reconstructions of the head phantoms** used as illustrations in this book.

4.4 Head Phantom with a Large Tumor and Local Inhomogeneities

In Fig. 4.5(a) we show an actual brain cross section. The left half of the image shows a malignant tumor that has a highly textured appearance. In order to simulate the occurrence of a similarly textured object in our phantom we need to use many additional elemental objects. This was done by adding to the list of elemental objects (Table 4.2) that produced Fig. 4.4 a much longer list of elemental objects, each coinciding exactly with a pixel; this resulted in the phantom shown in Fig. 4.5(b). Because of the medical relevance of imaging brains with such tumors, for the rest of this book we use the head phantom with this tumor added to it. (Due to our display method, it seems that there is a large range of values in the tumor. However, this is an illusion: the range of values in the tumor is less than 7% of the range of values in the picture that is displayed in Fig. 4.4. Another way of saying this is that the range of the difference between the pictures represented by Figs. 4.4 and 4.5(b), is less than 7% of the range within either of those pictures.)

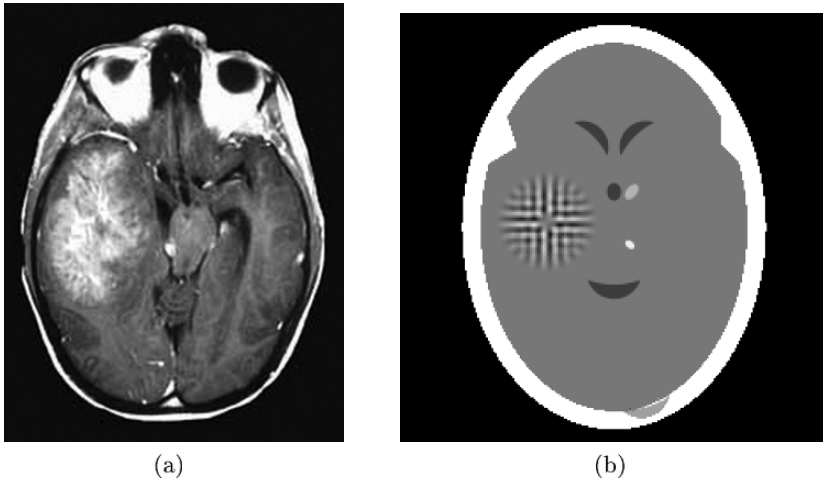(a)   (b)

Fig. 4.5: (a) An actual brain cross section with a tumor. (Image is reproduced, with permission, from the Roswell Park Cancer Institute website.) (b) The head phantom of Fig. 4.4 with a "large tumor" added to it.

(a)   (b)

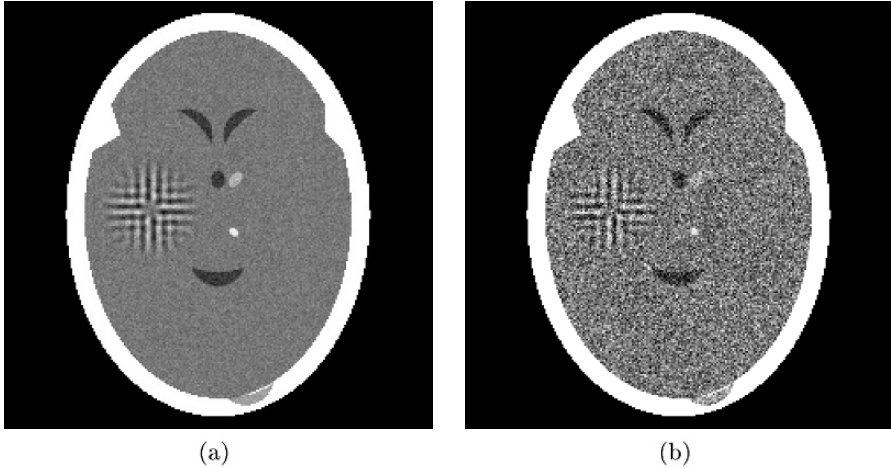Fig. 4.6: Head phantoms with local inhomogeneities. (a) $\sigma_X = 0.0025$. (b) $\sigma_X = 0.01$.

One problem with the phantoms as defined so far is that a brain is far from being homogeneous: it has gray matter, white matter, blood vessels and capillaries carrying oxygenated blood to and deoxygenated blood from the brain, etc. This is even more so for bone, whose strength to a large extent is derived from its structural properties (it is more like the Eiffel tower than a monolith of solid stone). There are methods that can obtain remarkably accurate reconstruction of piecewise homogeneous objects, but their performance may not be medically efficacious when applied to CT data from real objects with local inhomogeneities. So as not to fall into the trap of drawing too optimistic conclusions from experiments using piecewise homogeneous objects, we superimposed on our head phantom a random local variation that is obtained by picking, for each pixel and for each energy level, a sample from the Gaussian random variable X with mean $\mu_X = 1$ and a variance V_X that reflects the level of local inhomogeneity present in our object (see (1.10)) and then multiplying the previously estimated linear attenuation coefficient at that energy level with that sample. In Fig. 4.6 we show the results of this for 60 keV for two different values of $\sigma_X = \sqrt{V_X}$. The value that we use for the phantoms in the rest of this book is $\sigma_X = 0.0025$, shown in Fig. 4.6(a).

4.5 Creation of the Ray Sums

The simulation of the data collection in SNARK09 is based on (2.3):

$$p = -\ln\left(A_p/C_p\right). \tag{4.2}$$

We first discuss how the calibration measurement C_p is calculated. It is given by

$$C_p = C_0/C_r, \tag{4.3}$$

where C_0 is the number of photons counted by the detector under consideration and C_r is the number of photons counted during the same period by a reference detector. As discussed in Section 3.1, both C_0 and C_r are samples of Poisson random variables, which can be approximated by Gaussian random variables if their means are large. In SNARK09 it is assumed that C_0 and C_r are samples of the same Gaussian random variable (with a user-provided mean), and so the expected value of C_p is one. In fact, if the user of the programming system requests the simulation of the physically unattainable case of no error due to photon statistics, the value of C_p is taken to be exactly one. Otherwise, a random number generator is used to produce C_0 and C_r.

A subtle point is that, except in the case of the fifth scanning mode (Fig. 3.3(e)), C_p is not to be calculated separately for each source–detector pair. This is because of the way calibration is done in the different scanning modes (see Section 3.4). In the first two scanning modes (Figs. 3.3(a) and (b)), C_p is the same for all source–detector pair positions that are used to obtain data for one set of parallel lines. Similarly, in the fourth scanning mode (Fig. 3.3(d)), C_p is the same for all lines that diverge from the same detector as the source moves. The situation with the third scanning mode is essentially different: C_p is the same for all lines that connect the source to a particular detector as the apparatus moves. All these lines are tangential to the same circle, and this may cause a ringlike feature to appear in the reconstruction if an error has been made during the calibration measurement. (This artifact can be observed in Fig. 4.2, which was produced by an early CT scanner.)

We now turn to how the actual measurement A_p is calculated. It is given by

$$A_p = A_0/A_r, \tag{4.4}$$

where A_0 is the number of photons counted by the detector under consideration and A_r is the number of photons counted by the reference detector. Again A_r is taken to be a sample of a Poisson random variable with a user-provided mean, say λ. The calculation of A_0 is more complex since it is during this calculation that SNARK09 introduces polychromaticity, the shape of the x-ray beam, and scatter.

In order to understand this clearly, we have to go back to the way we create a phantom (Section 4.2). The phantom is put together from a number of elemental objects each with an associated density. Since the phantom represents the distribution of relative linear attenuation at a fixed energy, we need only one density associated with each elemental object. If we want to represent the relative linear attenuation at a different energy, we need to use different densities for the elemental objects. In order to describe the interaction of a polychromatic x-ray beam with the phantom, densities for all energies in the beam need to be given.

SNARK09 solves this problem as follows. It assumes that the x-ray spectrum is discrete; i.e., it consists of a mixture of photons that are of one of a finite number of different energies. For each energy the user has to specify the percentage of photons at that energy (based on the detected spectrum during the calibration measurement, see Section 3.2) and the density at that energy of all the elemental objects. (In general, the user also needs to specify the absorption properties of the reference material at the different energies, but since in our example the reference material is air we do not dwell on the details of this point.)

Since the density (in our case: relative linear attenuation at a fixed energy) at a point is the sum of the densities of all the elemental objects within which the point lies, the integral of the density along a line L is the sum over all elemental objects of the products of the length of intersection of L with the elemental object and the density in the elemental object.

Assume for now that we have a point source, a point detector, with a line L between them, and no scatter. Then (3.10), when combined with (4.2) and (4.4), yields

$$A_0 \simeq \lambda \int_0^E \tau_e \exp\left(-\int_0^D (\mu_e(z) - \mu_e^a)\, dz\right) de, \tag{4.5}$$

where we have made use of the assumptions that the expected values of C_p and A_r are 1 and λ, respectively. In SNARK09, the expression on the right-hand side of (4.5) is evaluated as follows.

Let I be the number of discrete energy levels and J be the number of elemental objects. Let $d_{j,i}$ be the density of the jth elemental object at energy level i, let ℓ_j be the length of intersection of the line L with the jth elemental object (ℓ_j may be 0), and let t_i be the probability that a photon counted during the calibration measurement is at energy level i (these probabilities are user specified). Then A_0 is taken to be a sample of a Poisson random variable with mean

$$\lambda \sum_{i=1}^I t_i \exp\left(-\sum_{j=1}^J \ell_j d_{j,i}\right). \tag{4.6}$$

If the user wishes to simulate the physically unattainable case of no photon statistics, SNARK09 sets A_0 equal to the value provided by (4.6). To simulate the shape of the x-ray beam, SNARK09 calculates A_0 as the weighted average of the values of (4.6) for a number of different lines between the source and the detector.

To simulate scatter, SNARK09 replaces the value A_0 for a detector position by a weighted average of the values of A_0 for that detector position and the neighboring detector positions. The scatter contribution of a detector position to another one is assumed to depend only on the distance between the two detector positions. Mathematically, we express this by saying that the values A_0 with scatter taken into consideration are obtained by *convolution* of the

values of A_0 without scatter and a fixed *scatter function*. (The notion of convolution, which is essential for some of the reconstruction algorithms, is explained in Section 8.1.) This model for the scattering process is a very much simplified version of what really happens; scatter simulated by SNARK09 resembles true physical scatter only in its gross characteristics.

In the next chapter we give examples of how SNARK09 simulates the different processes just described and of the effects of these processes on the quality of the reconstruction.

4.6 Fast Calculation of a Ray Sum for a Digitized Picture

As long as the number J of elemental objects composing a phantom is not particularly large, evaluating a formula such as the one that occurs in (4.6) is not computationally demanding: for each line, we loop through all the elemental objects j, and using the location and shape of the elemental object we calculate the length ℓ_j of the intersection of that line with that elemental object. However, the situation changes essentially by the introduction of local inhomogeneities. Mathematically, the introduction of local inhomogeneities can be thought of as just the introduction of extra elemental objects, one per pixel, with densities assigned to them that represent the calculated inhomogeneities at those pixels in the phantom, as described at the end of Section 4.4. However, the number of pixels tends to be large (in our head phantom it is 59,049) and to loop through all of them for each line would result in a considerable computational burden.

Fortunately, there is an alternative. Using an approach often referred to as a *digital difference analyzer* (*DDA*, for short), one can rapidly obtain, for each line, the location of all the pixels intersected by that line and the lengths of those intersections. Then the inner sum in (4.6) can be rapidly evaluated using only those pixels that are intersected by the line. Since typically only a small fraction of pixels is intersected by any line, this results in a very significant computational speedup. The same idea can be, and is, used in the implementation of the so-called series expansion reconstruction algorithms, discussed later in Section 6.3 and, in more detail, in Chapters 11 and 12.

The idea of a DDA for locating for a line L the pixels that are intersected by L and the lengths of the intersections is described in Fig. 4.7. Let us denote, as in Fig. 2.4, by θ the angle that L makes with the y (vertical) axis. We make two nonessential assumptions to simplify the presentation of the idea behind the DDA; it is easy to work out how the details of our presentation need to be changed if these nonessential assumptions are not satisfied. The assumptions are that $0 \leq \tan \theta < 1$ and that the point b where L "first" intersects the picture region lies on the top horizontal edge.

Given geometrical information about the location of the line, we can easily calculate the coordinates of the point b. We denote the length of a side of a
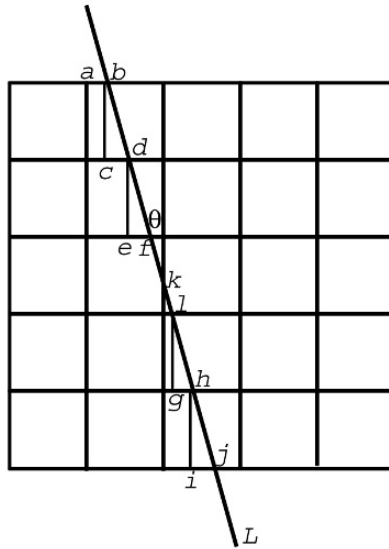
Fig. 4.7: A digital difference analyzer (DDA) for lines.

pixel in Fig. 4.7 (and hence also the distance between b and c, between d and e, between l and g, and between h and i) by δ. Let us abbreviate $\delta \tan \theta$ by τ and $\delta / \cos \theta$ by λ. Note that in Fig. 4.7, τ is the distance between c and d, between e and f, between g and h, and between i and j, while λ is the distance between b and d, between d and f, between l and h, and between h and j. In fact, λ is the length of intersection of L for four out of the six pixels that L intersects.

The control of the DDA is achieved by using a variable χ such that $0 \leq \chi < \delta$, which is initialized to be the distance between a and b. The DDA lists one-by-one each intersected pixel P, together with the length of intersection $l(P)$. The first P is the one that contains b.

The whole process can be understood by considering the general case of having a current value for χ and for P. We distinguish between two possibilities, and in either case the amount of computing that needs to be done is very little:

(i) $\chi + \tau < \delta$. In this case $l(P) = \lambda$, χ is replaced by $\chi + \tau$ and P is replaced by the pixel below it. The process stops if there is no such pixel.
(ii) $\chi + \tau \geq \delta$. In this case $l(P) = \lambda \frac{\delta - \chi}{\tau}$ and P is replaced by the pixel to the right of it. The process stops if there is no such pixel. For this new P,

$l(P) = \lambda^{\frac{\chi+\tau-\delta}{\tau}}$. Now χ is replaced by $\chi + \tau - \delta$ and P is replaced by the pixel below it. The process stops if there is no such pixel.

Unless the process has stopped due to the nonexistence of a looked-for pixel, we are now back to the general case and the same two possibilities are considered again. Clearly, the total process can be programmed in a very efficient manner.

Notes and References

SNARK09 is described in detail in [61].

The linear attenuation coefficients of the various tissue types (except for bone) at the different energies were estimated from the values published by [219]. Values for bone were estimated based on the assumption that it is a mixture of calcium and fat.

Head phantoms, which are less realistic than the one discussed in Section 4.2, were proposed in [138] and [241]. The latter of these is usually referred to as the Shepp–Logan head phantom and it has been extremely widely used for evaluating reconstruction algorithms. Nevertheless its use for this purpose is not really advisable, since it lacks anatomical features (such as nearly straight edges of bones) that are likely to deteriorate the clinical usefulness of reconstructions. Many dozens of mathematically described phantoms of various parts of the human body have been proposed since these early works, much of it on the Internet. A particularly rich source of phantoms was produced by FORBILD (the Bavarian Center of Excellence for Medical Imaging and Image Processing), see http://www.imp.uni-erlangen.de/phantoms/.

The exact method for creating the "large tumor" of Fig. 4.5(b) is described in [121]. This large tumor also happens to be a ghost (as defined in Section 15.4); it is invisible for 22 projection directions.

A pioneering DDA-based practical algorithm for drawing lines using a digital plotter is due to Bresenham [30]. Both DDAs in general and Bresenham's algorithm in particular are referred to in a considerable body of literature; a relatively recent example is [66].